Meta Antenna for Smart Agriculture to detect Red Palm Weevil in Palm trees.

Abstract

Palm tree infestations by the red palm weevil (RPW) pose significant economic challenges globally. Annually, Europe suffers losses amounting to several hundred million euros due to palm tree issues, with notable financial setbacks reported in Spain and Abu Dhabi. Although insecticides are effective, early detection remains a critical hurdle.

In this research paper, we introduce a pioneering approach using a custom-designed, non-invasive sensor for early detection of the red palm weevil (RPW) in palm trees. Our sensor exploits the difference in permittivity between palm tree tissues and RPW insects, resulting in distinct electromagnetic interaction patterns that can confirm the presence of the insect. This method was developed with the specific goal of detecting RPW but has the potential to detect other insect species by analysing variations in electromagnetic interactions.

Introduction

A) Red Palm Weevil

The red palm weevil (RPW), Rhynchophorus ferrugineus Olivier is indigenous to south and southeast Asia and spread to Africa and Europe later reached Mediterranean at late 1980s (Figure 1). Larvae of Rhynchophorus was a delicious of southeastern cuisine, however, larvae farming was prohibited to prevent the potential devastation of plantation crops [3].

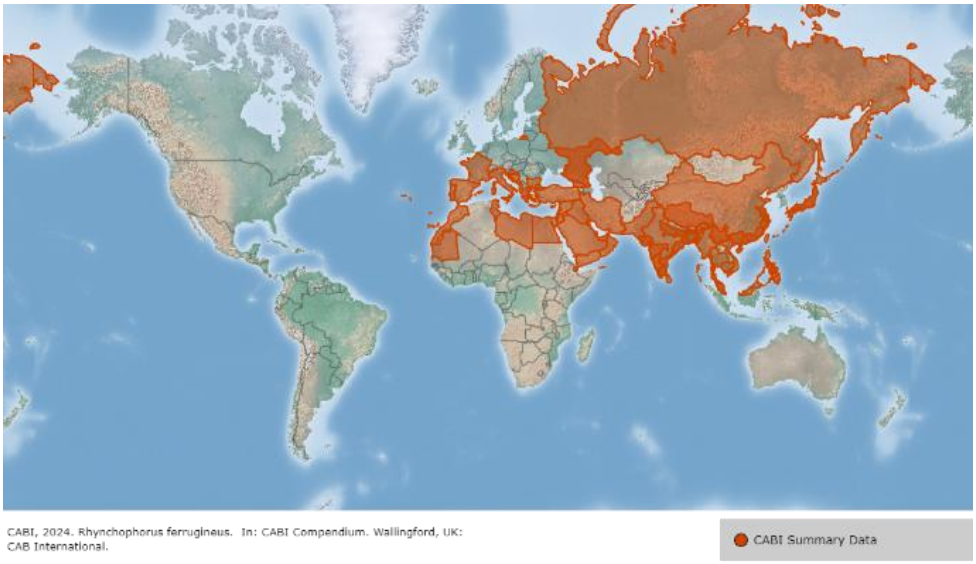

Figure 1 Geographic distribution of the red palm weevil, based on data from the Invasive Species Compendium. Available at https://www.cabi.org/isc/datasheet/47472

RPW, with a life cycle lasting three to four months, is attracted to fresh palm wounds' volatiles for egg laying. Gravid females deposit over 200 eggs in cracks on soft palm tissue, predominantly in young coconut and date palms below 20 years old. Oviposition is temperature-sensitive, influencing the number of generations per year. Larvae feed and migrate within the palm, with overlapping generations possible. In colder climates, one generation per year occurs below 15°C, while warmer climates see over two generations above 19°C. Larval stages can extend up to 160 days in the Mediterranean's

winter-spring seasons. Upon completing 7–16 instars, mature larvae pupate in fibrous cocoons, culminating in adult weevil emergence (Figure 2).

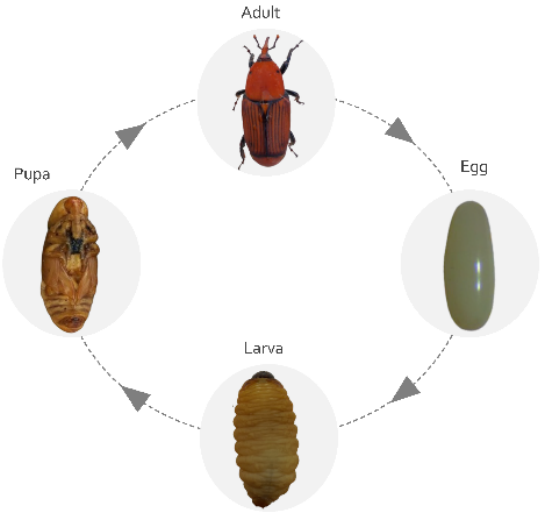

Figure 2 The life cycle stages of the red palm weevil, R. ferrugineus. Available at https://www.mdpi.com/2075-4450/14/3/255

B) Palm Tree

There are over 2,600 different type of palm trees belongs to Arecaceae family. It is one of the first plant to be harvested. Palm harvest is famous in many parts of the world, especially in Asia, Africa, and the Middle East (Table 1). These regions have the suitable climate and soil conditions for growing different types of palm trees [4,5,6,7]. These magnificent trees could grow 30 to 50 meters tall and 30 to 40 centimetres wide. A date tree can live for about 50 years on average. Around 200 days pass between pollination and fruit growth. The amount of fruit an adult tree produces might range from 20 to 100 kilograms, depending on the environment and cultivation methods.

Table 1 Leading countries in palm production.

Country	**Famous Palm**
Egypt	Date palm
Indonesia	Palm oil
Philippines	Coconuts
Madagascar	Raffia palm

C) Sensor Novelty

Various research studies have explored different methods for detecting the presence of red palm weevils (RPW). These methods include acoustic signal processing [8], optical distributed sensing [9,10], high-power microwave sensing, and thermal heating treatment procedures [11,12,13,14,15], among others. For instance, in a particular paper [16], a CSRR sensor was presented for classifying the gender of RPW, demonstrating an innovative application of sensor technology. Additionally, significant advancements in numerical simulation techniques for controlling RPWs were detailed in the paper [17]. In this work, the authors introduced a Finite-Difference time domain (FDTD) simulation model specifically tailored to assess the effectiveness of microwave energy for targeting RPWs. The simulation results highlighted that RPWs in the larval stage absorbed sufficient electromagnetic energy, leading to their extensive destruction.

Many analysis methods have been developed, but the most intriguing ones are those that are non-invasive and non-destructive to the material under test (MUT). Due to the thick cuticle layer, microwave signal propagation is affected, causing waves to reflect, absorb, or deviate from their path. To detect

variations in the dielectric nature of the red palm weevil (RPW), a novel small sensor based on complementary split-ring resonators (CSRR) has been designed and proposed in this paper. The study proposes using a circular patch microstrip antenna to measure the relative permittivity of different stages of palm tree health (healthy, partially damaged, and fully damaged) by incorporating a cut-out type CSRR in the resonant element. The permittivity values for RPW proposed in [17] and for the palm tree under various conditions mentioned in [18] are employed in this study.

Table 2 Permittivity of palm and RPW for [17,18].

Subject	**Dielectric value**
Healthy trunk	30.3
Partially healthy trunk	35.3
Highly infected trunk	50.7
RPW (larva)	32-36 (real)

Sensor Design.

Comparing different microwave cavity resonators and micro-cantilever-based sensors, planar microwave sensors are favored for their small size, ease of manufacture, low cost, and lightweight characteristics [19,20,21]. Open-ended half-wavelength resonators, known for their excellent quality factor and compact size, are adapted as Split Ring Resonators (SRR) and commonly used as sensing elements [22,23,24]. Planar sensors have been utilized in microfluidic systems for label-free biomolecule and concentration detection [25,26,27,28,29,30]. Complementary Split Ring Resonator (CSRR) structures have been employed to enhance accuracy and the minimal detectable limit in liquid media [31,32,33]. CSRRs also function as LC (Inductance-Capacitance) resonator tanks, where the inductance (L) is due to the current flow on the metal ring and the capacitance (C) arises from the cuts or slots between the adjacent metal rings.

$$f_t = \frac{1}{2\pi\sqrt{(L_t * C_t)}} \quad (1)$$

In equation (1), f_t represents the resonance frequency of the CSRR, and L_t and C_t denote the total inductance and capacitance of the CSRR. Complex permittivity can significantly impact the design of RF and microwave circuits, especially at high frequencies. Several examples of complex permittivity measurements using resonant-based sensors are demonstrated by utilizing substrate permittivity [34, 35, 36, 37].

In Reference [34], a cross-shaped microstrip ring operating at 880 MHz has been developed for substrate sensing of materials such as Teflon, R4003, FR4, RF35, and glass. The measured data are inverted to obtain actual values using an artificial neural network (ANN) as a post-processing step. Additionally, in Reference [38], a ring resonator operating at 2.4 GHz is utilized to measure the moisture content of sand or concrete grains. This highly sensitive sensor boasts a small size and high accuracy as key features.

A) Meta Sensor

The proposed sensor operates in a narrow band at 4.8 GHz in free space. In the presence of the red palm weevil (RPW), resonance frequency undergoes a significant shift. The process of formulating the design, or the procedural steps, will be elucidated by detailing how the sensor arrived at this specific design systematically. Initially, a circular planar sensor with a radius of 31.29 mm was tested to observe a frequency shift of 1MHz. A mirror-symmetric Complementary Split Ring Resonator (CSRR) was then etched at the centre of the circular element to enhance accuracy and sensing capability. This design

approach was inspired by a cross-shaped microstrip sensor discussed in Reference [34], which demonstrated improved measurement of the complex permittivity of solid materials.

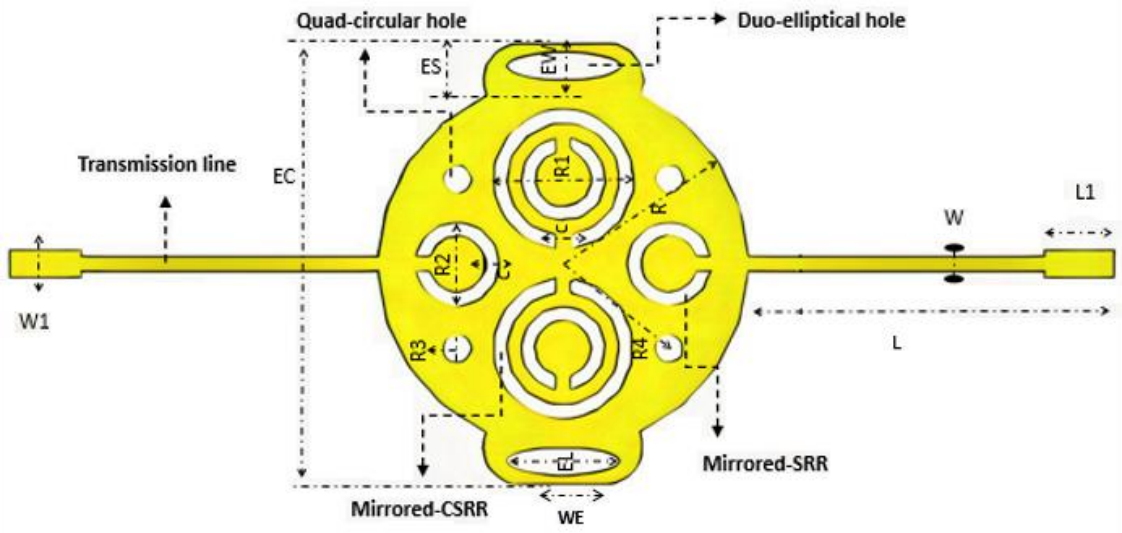

Figure 3 : Structural design of DUO-DUPLET CSRR-BASED MICROWAVE SENSOR

Table 3: Designing parameter of DUO-DUPLET CSRR-BASED MICROWAVE SENSOR.

Details	**Marking**	**Dimension (mm)**
Length of Transmission line	L	25.94
Width of Transformer line	W	1.00
Length of Microstrip line	L1	5.00
Radius of the inner core circle	R	13.11
Diameter of the complementary split ring circle	R1	10.00
Diameter of the split ring circle	R2	6.00
Diameter of the circular slot	R3	2.00
Distance from origin of inner core to the circular slot	R4	8.20
Distance of the circular slot	C	1.00
Width of the elliptical bud	ES	3.71
Width of the duo elliptical bud	EW	2.00
Length of the outer elliptical bud	WE	5.11
Width of the core sensor	EC	31.29
Width of Microstrip line	W1	2.00
Length of the duo elliptical bud	EL	8.00

For our specific application, we propose a model that involves a cross-shaped structure and dual elliptical bud. These configurations are placed at both external ends of the circular element, resulting in increased sensitivity and a significant improvement in frequency shift (as indicated in Table 4). To enhance accuracy further, circular holes and rings were etched at specific locations. We used an FR-4 substrate with a thickness of 0.158 cm, dielectric constant of 4.4, and loss tangent of 0.02.

Table 4: Difference in frequency shift (A) with and (B) without the presence of MUT at different steps of design.

Sensor Models	Resonance Frequency		dB
	A	B	
Plane sensor	5.333	5.3331	-53.394
CSRR proposed	4.633	4.633	-55.557
C & E hole	4.843	4.8709	-69.691
CSRR & design	4.857	4.808	-100.85

Principle of Operation and Sensitivity

In microwave resonators, when operating at the resonant frequency, the energy stored in both the electric and magnetic fields within the structure must be equal. As a result, Equation (1), which establishes the relationship between the permeability and permittivity of the medium and the resonant frequency of the element, can be employed to extract information about the properties of external materials. These materials can introduce disturbances when they interact with the electromagnetic field [39].

$$\frac{\Delta f_r}{f_r} = \frac{\int_v (\Delta\varepsilon E_1 . E_o + \Delta\mu H_1 . H_0) dv}{\int_v (\varepsilon_o |E_o|^2 + \mu_o |H_o|^2) dv} \qquad (1)$$

In Equation (3), Δf corresponds to the observed variation in the resonant frequency, f; $\Delta\varepsilon$ represents the change in relative permittivity; $\Delta\mu$ denotes the change in magnetic permeability; and ε and μ refer to the permittivity and permeability of free space, respectively. Additionally, E and H signify the distributions of electrical and magnetic fields, respectively, in the absence of external disturbances. Conversely, E' and H' represent the corresponding distributions of electrical and magnetic fields when external disturbances are present. The parameter v represents the volume affected by these disturbances, specifically the cavity region in contact with the material under test (MUT).

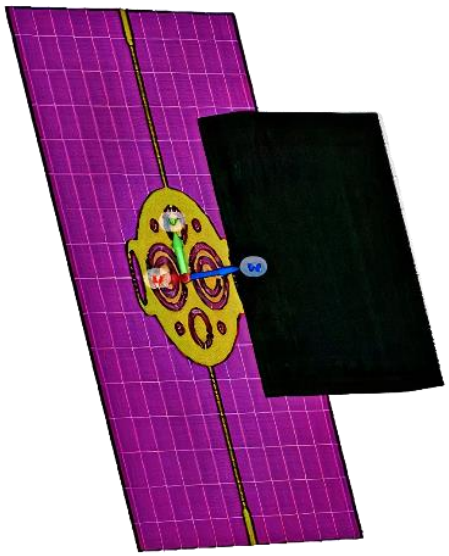

Figure 4 : Duo-duplet CSRR sensor with cubical MUT

Similarly, the capacitance between the ends of the resonator element exhibits significant dependency on the permittivity of the surrounding medium. Likewise, the induced current in the resonator element is directly influenced by the medium's permeability. This characteristic makes CSRR elements particularly sensitive to changes in the permittivity of the medium in which they are embedded, validating the application of CSRR in the proposed sensor geometry.

The characterization of various materials using the proposed sensor involved inserting separate samples of these materials into a container positioned over the microstrip antenna's patch. The sensor structure is simulated with material samples using CST Studio Suite software.

In the simulation, the relative permittivity ε_r of the material under test (MUT) varied from 30 to 50 in steps of five. The cube dimensions are 40 mm in length, 40 mm in width, and 5 mm in height. The simulated results for the variation of the proposed antenna's permittivity are illustrated in Graph 1. In the carried-out simulation, dielectric losses are neglected.

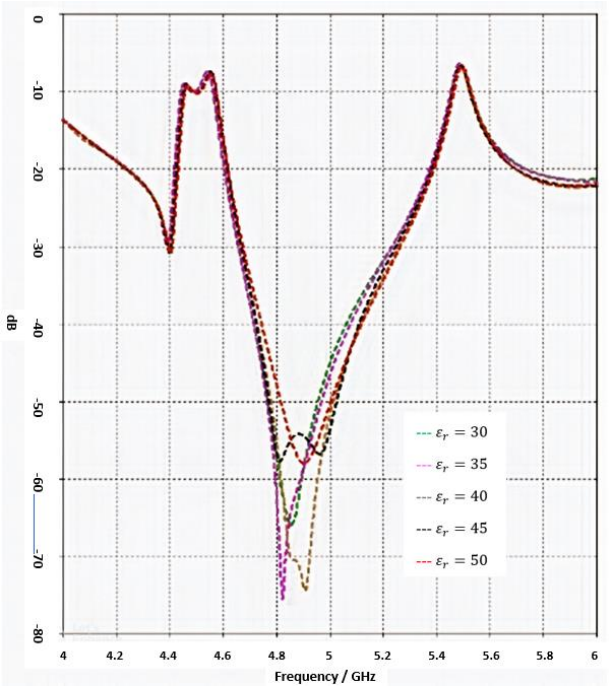

Graph 1 : Reflection coefficient, S11 (dB), results for different (MUT) relative permittivity's values at resonant frequencies.

The sensitivity of the proposed sensor (shown in Fig 3) was evaluated for each material under test (MUT) by analysing the variations observed in resonant frequency, according to Equation (2).

$$S = \frac{f - f_r}{\varepsilon_r - 1} \qquad (2)$$

Where f_r is the resonant frequency of the proposed sensor with the material under test (MUT) samples, f is the resonant frequency of the proposed sensor without MUT samples, and ε_r is the relative permittivity of the MUT samples. The sensitivity of the proposed sensor is calculated using Equation (2), and the corresponding outcomes are visualized in Graph 2.

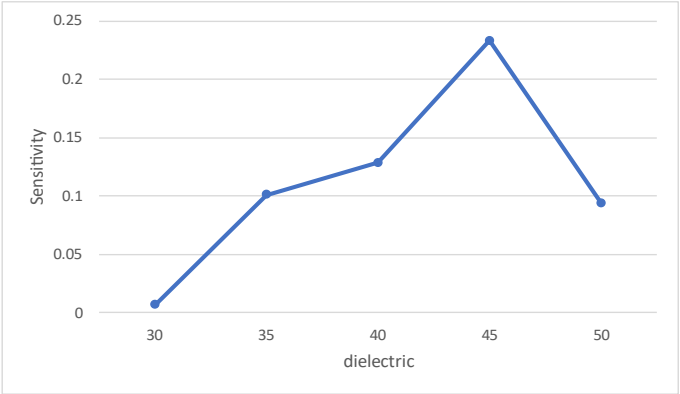

Graph 2 : Sensitivity(S) vs Dielectric

Result

The simulation results for the S-parameter obtained from CST Studio Suite for the proposed sensor show a dip of -100.85 dB at 4.857 GHz for S21(Graph 3), which helps analyse the variation of a dielectric substance placed before the sensor. By comparing the changes in frequency and dB, significant variations in the graph could be observed as the dielectric value changes.

The dielectric value, also known as the dielectric constant or relative permittivity, is a measure of a material's ability to store electrical energy in an electric field and it is a dimensionless quantity. The dielectric value indicates how easily a material can be polarized by an electric field. It is an important parameter in various electrical and electronic applications, including capacitors, transmission lines, and insulators.

Different materials exhibit different dielectric values, which can extend from very low (e.g., vacuum or air) to very high (e.g., certain ceramics and plastics). Table 2 represents the dielectric values of palm trees at different stages of red palm weevil (RPW) infestation, indicating the presence of RPW and the damage it causes.

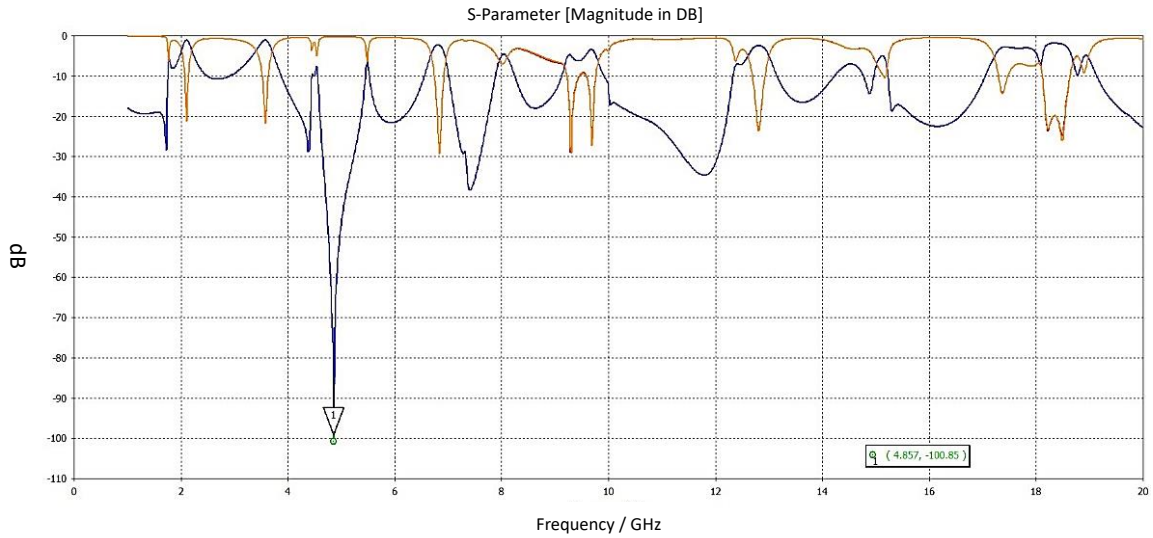

Graph 3 : S-parameter (S21) without MUT.

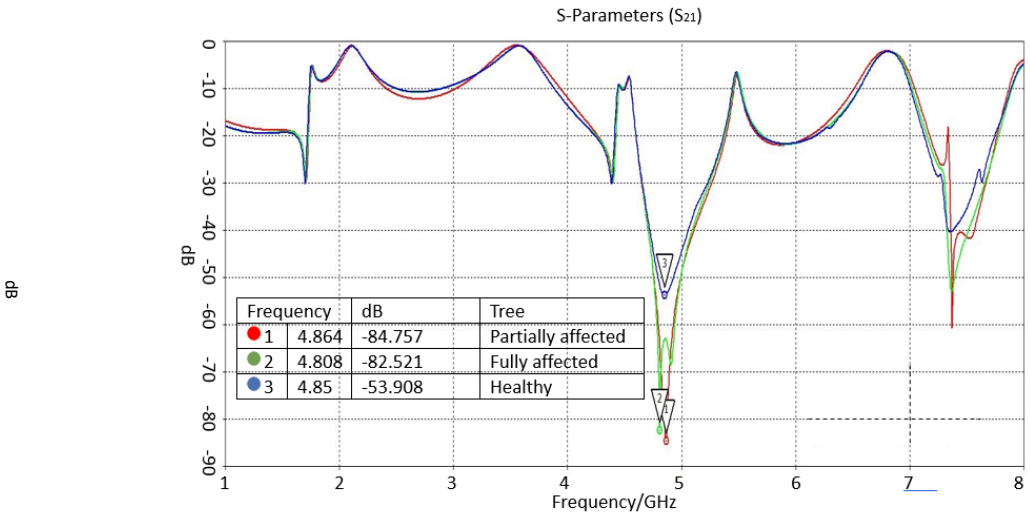

Graph 4 : The distance between the sensor and the trunk is 14mm and variation in its S-parameter. Red for partially affected, Green for fully affected, Blue for healthy trunk.

Table 5 : This table provides the respective value derived from Graph 4. Δfrequency is calculated by subtracting the resonance frequency without and with MUT.

Trunk	ε_r	f (GHz)	Δf (GHz)	**dB**	**ΔdB**
Healthy	30.3	4.85	-0.007	-53.908	46.94
Partially healthy	35.3	4.864	0.007	-84.757	16.09
Highly infected	50.7	4.808	0.049	-82.521	18.32

The sensor readings were taken at distances of 14mm and 30mm from the infected portion, which exhibited varying degrees of infestation. The modifications in sensor readings are depicted in Graphs (4-5) and summarized in Tables (5-6). The variations in resonance frequency and dB (power) change according to the distance and the dielectric value of the material under test (MUT). This is demonstrated and discussed in detail in this paper.

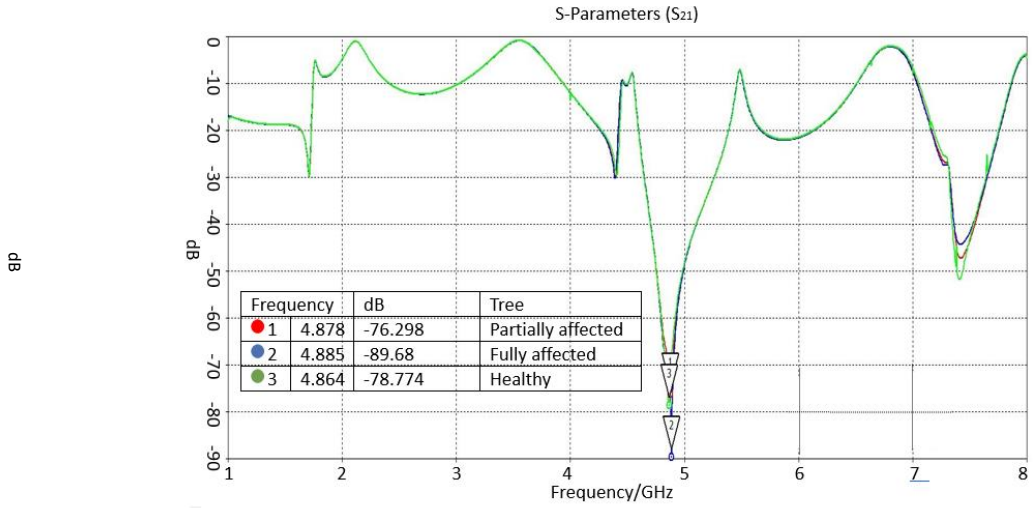

Graph 5 : The distance between the sensor and the trunk is 30mm and variation on its S parameter. Red for partially affected, Green for fully affected, Blue for healthy.

Table 6 : This table provides the respective value derived from Graph 5. Δfrequency is calculated by subtracting the resonance frequency without and with MUT.

Trunk	ε_r	f (GHz)	Δf (GHz)	**dB**	**ΔdB**
Healthy	30.3	4.864	0.007	-78.774	22.07
Partially healthy	35.3	4.878	0.021	-76.298	24.55
Highly infected	50.7	4.885	0.028	-89.68	11.17

In the simulated plot above, you can observe two peaks changing their status when examined under different environmental conditions. The relationship between these peaks and the distance from the palm tree provides insight into the degree of infestation caused by the red palm weevil (RPW) in the palm tree. These simulations demonstrate the potential of using sensor data to assess the level of infestation by RPW. Flow Chart (1) outlines the process mechanism for detecting the presence of the red palm weevil (RPW).

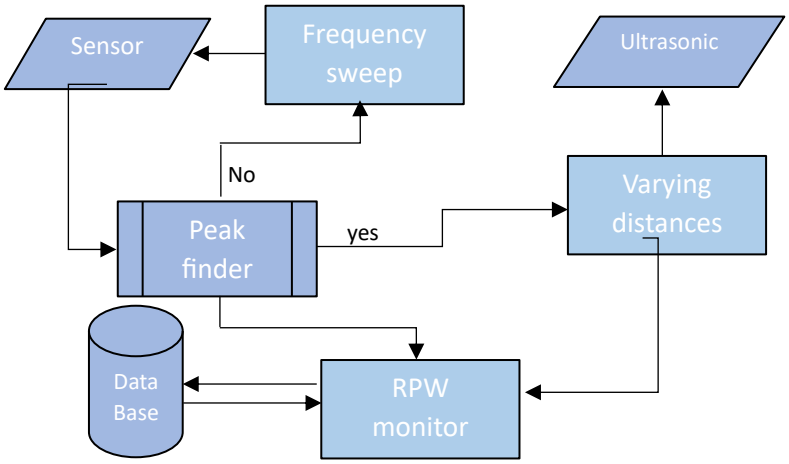

Flow Chart 1 : Detection mechanism

By using frequency sweep, we can identify peaks at specific steps, and repeating the sweep for the same distance can provide us with an average peak. Data collected at different frequencies and distances using this method can be used to detect the presence of the red palm weevil (RPW).

Conclusion

A new, compact microwave sensor has been designed to detect the presence of the red palm weevil (RPW). This sensor features a circular microstrip patch antenna with two slotted complementary split-ring resonators (CSRRs). The operational principle involves comparing the signal strength at different distances from the palm tree. This task can be performed manually, or unmanned aerial vehicles (UAVs) can also be used to carry out the detection process, as the sensor consumes very little power. The developed sensor has significant potential and can be applied in various scenarios due to its affordability, lightweight construction, and ease of manufacturing.

Figure (5) displays the surface current distribution on the sensor. The electron flow density in the DUO-duplet CSRR confirms the operation of all CSRR components within the resonator. The collective interaction of these sensor components contributes to the observed results.

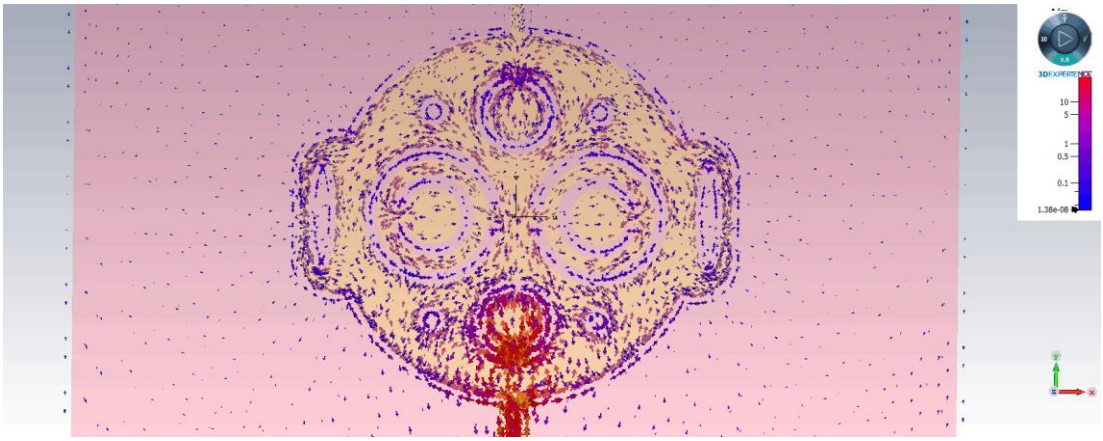

Figure 5 : Surface current

With this sensor, the presence of red palm weevil (RPW) can be detected. Using techniques such as peak detection and clustering can even allow for determining how many red palm weevils are present at a specific location on the palm tree.

The smaller size of this sensor allows for integration into a printed circuit board (PCB) to create a Monolithic Microwave Integrated Circuit (MMIC) for a portable, non-destructive red palm weevil detector. Unlike traditional integrated circuits created using silicon technology, MMICs are created using a specialized semiconductor process optimized for high-frequency applications. This process facilitates the integration of various microwave components, including amplifiers, mixers, and oscillators, onto a single chip. The result is a compact, lightweight, and high-performance circuit capable of operating at high frequencies.

Therefore, we conclude that this sensor could be a highly attractive option for detecting red palm weevil compared to all other conventional methods available in the market.

Reference

[1]. "ProQuest Document View." ProQuest, https://www.proquest.com/docview/2531380246/DE6718CCDA0B4D60PQ/3?accountid=31785&sourcetype=Scholarly%20Journals.

[2]. "ProQuest Document View." ProQuest, https://www.proquest.com/docview/1929501969/fulltext/DE6718CCDA0B4D60PQ/5?accountid=31785&sourcetype=Newspapers.

[3]. "Chỉ thị 01/2015/CT-UBND nghiêm cấm nhân nuôi phát tán đuông dừa tỉnh Bến Tre". Thư Viện Pháp Luật, retrieved 2022-01-05.

[4]. Kidadl. "Date Palm Tree Facts: From Cultivation to Harvesting the Fruit." Kidadl, https://kidadl.com/facts/history-geography-social-studies/date-palm-tree-facts-from-cultivation-to-harvesting-the-fruit.

[5]. Natural History Museum. "Date Palm: The Cornerstone of Civilisation in the Middle East and North Africa." Natural History Museum, https://www.nhm.ac.uk/discover/date-palm-the-cornerstone-of-civilisation.html.

[6]. Vivid Maps. "Which Country Has the Most Palm Species?" Vivid Maps, https://vividmaps.com/palm-species/.

[7]. WorldAtlas. "Leading Countries Growing Dates (Fresh Date Palm Fruits)." WorldAtlas, https://www.worldatlas.com/articles/world-leading-countries-growing-fresh-dates.html.

[8]. Nangai, V., & Martin, B. (2017). Interpreting the acoustic characteristics of RPW towards its detection—A review. *IOP Conference Series: Materials Science and Engineering, 225*, 012178. [Google Scholar] [CrossRef]

[9]. Ashry, I., Mao, Y., Al-Fehaid, Y., Al-Shawaf, A., Al-Bagshi, M., Al-Brahim, S., Ng, T.K., & Ooi, B.S. (2020). Early detection of red palm weevil using distributed optical sensor. *Scientific Reports, 10*, 3155. [Google Scholar] [CrossRef] [PubMed]

[10]. Wang, B., Mao, Y., Ashry, I., Al-Fehaid, Y., Al-Shawaf, A., Ng, T.K., & Ooi, C.Y.S. (2021). Towards detecting red palm weevil using machine learning and fiber optic distributed acoustic sensing. *Sensors, 21*(1592). [Google Scholar] [CrossRef] [PubMed]

[11]. Massa, R., Panariello, G., Pinchera, D., Schettino, F., Caprio, E., Griffo, R., & Migliore, M.D. (2017). Experimental and numerical evaluations on palm microwave heating for red palm weevil pest control. *Scientific Reports, 7*, 45299. [Google Scholar] [CrossRef] [PubMed]

[12]. Bini, M., Andreuccetti, D., Ignesti, A., Olmi, R., Priori, S., & Vanni, R. (1997). A portable microwave system for woodworm disinfestation of artistic painted boards. *Journal of Microwave Power and Electromagnetic Energy, 32*, 180–187. [Google Scholar]

[13]. Ali, I., Al-Jabr, A., & Memari, A. (2010). FDTD simulation and experimental investigation of controlled microwave irradiation of red palm weevils. *Proceedings of the IEEE Middle East Conference on Antennas and Propagation, Cairo, Egypt*, 20–22 October 2010, pp. 1–8. [Google Scholar]

[14]. Rmili, H., Alkhalifeh, K., Zarouan, M., Zouch, W., & Islam, M.T. (2020). Numerical analysis of the microwave treatment of palm trees infested with the red palm weevil pest by using a circular array of vivaldi antennas. *IEEE Access, 8*, 152342–152350. [Google Scholar] [CrossRef]

[15]. Bait-Suwailam, M.M. (2021). Numerical assessment of red palm weevil detection mechanism in palm trees using CSRR microwave sensors. *Progress in Electromagnetics Research Letters, 100*, 63–71. [Google Scholar] [CrossRef]

[16]. Bait-Suwailam, M.M. (2023). Towards Monitoring and Identification of Red Palm Weevil Gender Using Microwave CSRR-Loaded TL Sensors. *Sensors, 23*(6798). https://doi.org/10.3390/s23156798

[17]. Ali, I.A., Al-Jabr, A., & Memari, A.R. (2010). FDTD simulation and experimental investigation of controlled microwave irradiation of red palm weevils. *IEEE Middle East Conference on Antennas and Propagation (MECAP 2010), Cairo, Egypt*, 2010, pp. 1-8. doi: 10.1109/MECAP.2010.5724200.

[18]. Detection of Red Palm Weevil Infestation in Palm Trees. ASEE paper id #35900.

[19]. Ebrahimi, A., Withayachumnankul, W., Al-Sarawi, S.F., & Abbott, D. (2015). Microwave microfluidic sensor for determination of glucose concentration in water. *IEEE 15th Mediterranean Microwave Symposium (MMS)*, pp. 1–3.

[20]. Zhao, Y., Li, Y., Pan, B., Kim, S.-H., Liu, Z., Tentzeris, M.M., Papapolymerou, J., & Allen, M.G. (2010). RF evanescent-mode cavity resonator for passive wireless sensor applications. *Sensors and Actuators A: Physical, 161*(1–2), 322–328.

[21]. Vashist, S. (2007). A review of microcantilevers for sensing applications. *Journal of Nanotechnology, 3*(June), 1–15.

[22]. Wang, B., Long, J., & Teo, K.H. (2016). Multi-Channel Capacitive Sensor Arrays. *Sensors, 16*(2), 150.

[23]. Grenier, K., Dubuc, D., Poleni, P.-E., Kumemura, M., Toshiyoshi, H., Fujii, T., & Fujita, H. (2009). Integrated Broadband Microwave and Microfluidic Sensor Dedicated to Bioengineering. *IEEE Transactions on Microwave Theory and Techniques, 57*(12), 3246–3253.

[24]. Horestani, A.K., Fumeaux, C., Al-Sarawi, S.F., & Abbott, D. (2013). Displacement Sensor Based on Diamond-Shaped Tapered Split Ring Resonator. *IEEE Sensors Journal, 13*(4), 1153–1160.

[25]. Ebrahimi, A., Withayachumnankul, W., Al-Sarawi, S., & Abbott, D. (2014). High-Sensitivity Metamaterial-Inspired Sensor for Microfluidic Dielectric Characterization. *IEEE Sensors Journal, 14*(5), 1345–1351.

[26]. Lee, H.-J., Lee, H.-S., Yoo, K.-H., & Yook, J.-G. (2010). DNA sensing using split-ring resonator alone at microwave regime. *Journal of Applied Physics, 108*(1), 14908.

[27]. Lee, H.-J., Lee, J.-H., Choi, S., Jang, I.-S., Choi, J.-S., & Jung, H.-I. (2013). Asymmetric split-ring resonator-based biosensor for detection of label-free stress biomarkers. *Applied Physics Letters, 103*(5), 53702.

[28]. Lee, H.-J., Lee, J.-H., & Jung, H.-I. (2011). A symmetric metamaterial element-based RF biosensor for rapid and label-free detection. *Applied Physics Letters, 99*(16), 163703.

[29]. Rowe, D.J., Al-Malki, S., Abduljabar, A.A., Porch, A., Barrow, D.A., & Allender, C.J. (2014). Improved Split-Ring Resonator for Microfluidic Sensing. *IEEE Transactions on Microwave Theory and Techniques, 62*(3), 689–699.

[30]. Kapilevich, B., & Litvak, B. (2011). Optimized Microwave Sensor for Online Concentration Measurements of Binary Liquid Mixtures. *IEEE Sensors Journal, 11*(10), 2611–2616.

[31]. Lee, C.-S., & Yang, C.-L. (2014). Thickness and Permittivity Measurement in Multi-Layered Dielectric Structures Using Complementary Split-Ring Resonators. *IEEE Sensors Journal, 14*(3), 695–700.

[32]. Boybay, M.S., & Ramahi, O.M. (2012). Material Characterization Using Complementary Split-Ring Resonators. *IEEE Transactions on Instrumentation and Measurement*, pp. 1–9.

[33]. Naqui, J. (2016). On the Symmetry Properties of Resonator-Loaded Transmission Lines. In *Symmetry Properties in Transmission Lines Loaded with Electrically Small Resonators*, Springer, pp. 73–124.

[34]. Biffi Gentili, G., Avitabile, G., Cerretelli, M., Riminesi, C., & Sottani, N. (2002). Microwave permittivity measurements through cross-shaped ring sensors. In *2nd ISA/IEEE Sensors for Industry Conference*, pp. 208–211.

[35]. Fratticcioli, E., Dionigi, M., & Sorrentino, R. (2004). A Simple and Low-Cost Measurement System for the Complex Permittivity Characterization of Materials. *IEEE Transactions on Instrumentation and Measurement, 53*(4), 1071–1077.

[36]. Fratticcioli, E., Dionigi, M., & Sorrentino, R. (2002). A planar resonant sensor for the complex permittivity characterization of materials. In *IEEE MTT-S International Microwave Symposium Digest* (Cat. No.02CH37278).

[37]. Skulski, J., & Galwas, B.A. (1998). Planar resonator sensor for moisture measurements. In *12th International Conference on Microwaves and Radar. MIKON-98. Conference Proceedings* (IEEE Cat. No.98EX195).

[38]. Oliveira, J.G.D., Pinto, E.N.M.G., Silva Neto, V.P., & D'Assunção, A.G. (2020). CSRR-Based Microwave Sensor for Dielectric Materials Characterization Applied to Soil Water Content Determination. *Sensors, 20*(255). https://doi.org/10.3390/s20010255

[39]. Ansari, M.A.H., Jha, A.K., & Akhtar, M.J. (2015). Design and application of the CSRR-based planar sensor for noninvasive measurement of complex permittivity. *IEEE Sensors Journal, 15*, 7181–7189.